Cell Cycle 14:18, 2891–2898; September 15, 2015; © 2015 Taylor & Francis Group, LLC

Properties of cells through life and death – an acoustic microscopy investigation

Maurice M Pasternak[1], Eric M Strohm[2], Elizabeth SL Berndl[2], and Michael C Kolios[2,*]

[1]Sunnybrook Research Institute; Department of Physical Sciences; Sunnybrook Health Sciences Center; Toronto, ON Canada; [2]Ryerson University; Department of Physics; Toronto, ON Canada

Keywords: acoustic microscopy, adiabatic bulk modulus, apoptosis, attenuation, cellular proliferation

Current methods to evaluate the status of a cell are largely focused on fluorescent identification of molecular biomarkers. The invasive nature of these methods – requiring either fixation, chemical dyes, genetic alteration, or a combination of these – prevents subsequent analysis of samples. In light of this limitation, studies have considered the use of physical markers to differentiate cell stages. Acoustic microscopy is an ultrahigh frequency (>100 MHz) ultrasound technology that can be used to calculate the mechanical and physical properties of biological cells in real-time, thereby evaluating cell stage in live cells without invasive biomarker evaluation. Using acoustic microscopy, MCF-7 human breast adenocarcinoma cells within the G1, G2, and metaphase phases of the proliferative cell cycle, in addition to early and late programmed cell death, were examined. Physical properties calculated include the cell height, sound speed, acoustic impedance, cell density, adiabatic bulk modulus, and the ultrasonic attenuation. A total of 290 cells were measured, 58 from each cell phase, assessed using fluorescent and phase contrast microscopy. Cells actively progressing from G1 to metaphase were marked by a 28% decrease in attenuation, in contrast to the induction of apoptosis from G1, which was marked by a significant 81% increase in attenuation. Furthermore late apoptotic cells separated into 2 distinct groups based on ultrasound attenuation, suggesting that presently-unidentified sub-stages may exist within late apoptosis. A methodology has been implemented for the identification of cell stages without the use of chemical dyes, fixation, or genetic manipulation.

Introduction

There has been growing evidence that the physiological processes of proliferation and apoptosis share common genes and morphological features.[1] These commonalities are also seen in tumors, which often feature genetic changes that suppress apoptosis and promote cellular proliferation.[2] The differentiation between tumor cells actively proliferating and those committed to apoptosis is important to the study of cancer. The use of stains such as the combination of Hoescht 33342, propidium iodide and fluorescent anti-cyclin antibody[3] can allow for a multi-parametric cell death and cell cycle analysis. However, these protocols are limited by requiring the sample to be fixed, thereby preventing live cell analysis. Additionally, non-stem cancer cells are incapable of effluxing certain DNA-intercalating dyes, such as Hoescht 33342,[4] commonly used for live cell cycle analysis. This makes the use of such dyes inappropriate for long-term study of the same cell sample. Newer techniques have circumvented these limitations through genetic modification of cells to express fluorescent proteins fused to markers of the cell cycle,[5] but these approaches carry the risk of altering the function of cancer cells.[6]

It has been proposed that the physical and mechanical properties of cells may be effective alternatives to using biochemical or genetic markers for cell staging.[7] Cellular processes involve vast reorganization of components, which is reflected through changes in the mechanical properties of the cell.[8] Within proliferation, these processes include the duplication of genetic material in Synthesis between Growth 1 (G1) and Growth 2 (G2),[9] the dissolution of the nucleus by phosphorylation of nuclear lamins,[10] the morphological shift of the cell into a geometrically-round shape,[11] and the intracellular reorganization of organelles.[12] Programmed cell death, consisting of early and late stages,[13] is also marked by a series of controlled events,[14] including cell rounding, cellular blebbing, fragmentation into apoptotic bodies, and eventual phagocytosis by immune cells.[15]

Methods that measure changes in physical and mechanical properties include microrheology,[16] atomic force microscopy,[17] cell poking,[18] microplate manipulation,[19] and others.[20] However, these techniques are invasive and the resulting data may be influenced by the measurement procedure itself. To avoid this influence, an alternate methodology must be applied that probes the cellular properties non-invasively. Scanning acoustic microscopy offers a non-invasive and real-time alternative method of measuring physical cell properties.

Acoustic microscopy utilizes ultrahigh frequency ultrasound to detect characteristic changes in the absorption and reflection of sound waves passing through cells and tissues. These changes

*Correspondence to: Michael C Kolios; Email: mkolios@ryerson.ca
Submitted: 02/24/2015; Revised: 06/28/2015; Accepted: 07/01/2015
http://dx.doi.org/10.1080/15384101.2015.1069925

can be used to calculate physical and mechanical characteristics, including cell height, the speed of sound through cell compartments, the acoustic impedance, the cell density, the adiabatic bulk modulus, and the acoustic attenuation. Acoustic microscopy can measure these properties in live cells non-invasively and without using stains. To achieve cellular resolution, very high ultrasound frequencies are required to achieve wavelengths of the order of microns. Clinical ultrasound uses sound waves in the 1–10 MHz range and has a resolution of 0.2–1.0 mm, and a maximum penetration of about 15 cm. High frequency ultrasound, used predominantly in pre-clinical imaging of small animals, uses frequencies in the 20 MHz to 60 MHz range with up to 1–2 cm penetration and 20–30 μm resolution. Ultrahigh frequency ultrasound uses 100 MHz to 1 GHz frequencies, with resolutions approaching 1 μm at 1 GHz. Previous investigations of acoustic microscopy of proliferating cells were limited to imaging of mitotic spindle fibers and no quantitative analysis was performed.[21] Other studies that examined the ultrasound properties of apoptotic cells reported an increased ultrasound backscatter at 20 to 60 MHz,[22,23] and an increase in attenuation when performed at 375 MHz.[24] However, because measurements in the 20–60 MHz range have insufficient resolution to identify properties of individual cells, it is impossible to ascertain subcellular detail. Additionally, the studies at 20–60 MHz did not take into account whether observed changes in ultrasound characteristics were during early or late apoptosis.

In this study, acoustic microscopy was used as a means of non-invasively discriminating live cells within G1, G2, metaphase, early apoptosis, or late apoptosis without the use of any genetic manipulation or exogenous biomarkers. A description of signal processing methods used to extract the physical and acoustic properties are described in references 24–26. Key aspects of the method are also summarized in the supplementary section.[25,26]

Results

Cell visualization

Visualization of cyclin D1 and cyclin B1 in G1 and G2 phases in MCF-7 cells, respectively, was determined by immunofluorescence. Lovastatin-treated G1 cells displayed a dendrite-like morphology (**Fig. 1A and F**), extending protrusions to maintain adherence to the substratum. In contrast, G2 cells displayed increased cell size (**Fig. 1B and G**), with protrusions still visible, but with the expansion of the plasma membrane broadening the arms of these extensions.

MCF-7 cells in metaphase displayed a rounded morphology under phase contrast imaging (**Fig. 1C**). Additionally, the alignment of condensed chromatin in metaphase cells was observed through staining of DNA (**Fig. 1H**). Increased basal light exposure was also observed in the phase contrast images of early and late apoptotic cells (**Fig. 1D and E**), indicating that these cells also displayed a lessened adherence to the glass substrate, similar to other studies.[27,28] Additionally, these early and late apoptotic cells also exhibited cell blebbing, a common marker of classical apoptosis.[15] Exposed phosphatidylserine and nuclear chromatin were observed through Annexin V and propidium iodide staining, respectively (**Fig. 1I and J**).

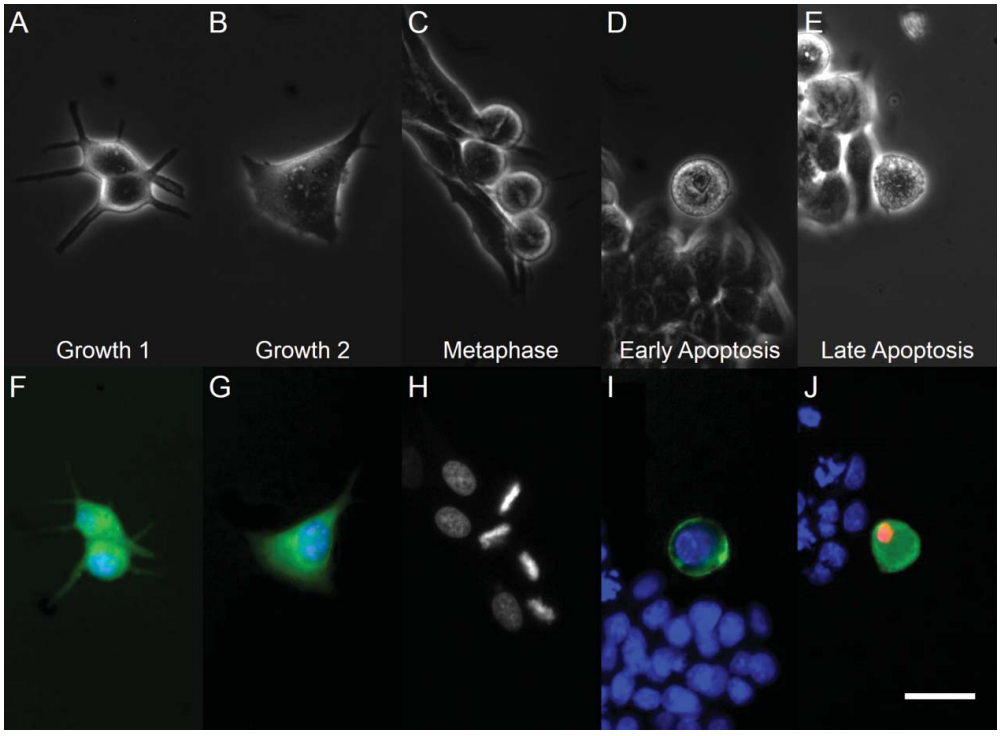

Figure 1. Light microscopy (top row) and fluorescent microscopy (bottom row) images of cells in different phases of the cell cycle and apoptosis. From left to right, panels correspond to G1, G2, metaphase, early apoptotic, and late apoptotic cells. Panel (H) has retained grayscale coloring for easier visualization of chromosome alignment on a dark background. White bar indicates 20 μm.

Ultrasound measurements

The cell height, sound speed, acoustic impedance, density, adiabatic bulk modulus and attenuation for each phase of the cell cycle are shown in **Table 1**.

The cell height (**Fig. 2A**) increased as cells progressed through the proliferative cell cycle, starting at G1. Values increased from 9.4 ± 1.5 μm for G1 to 11.4 ± 1.7 μm for G2, further increasing to 19.4 ± 2.5 μm for metaphase cells. Commitment to apoptosis results in a highly significant

Table 1. Quantitative values of physical acoustic properties. Mean values along with standard deviations of the measured properties are provided for proliferating cells (G1, G2, metaphase) and apoptotic cells (early and late apoptosis), with water serving as a reference. N = 58 for each group.

Cell State	Cell Height (μm)	Sound Speed (m/s)	Acoustic Impedance (MRayls)	Density (kg/m^3)	Adiabatic Bulk Modulus (GPa)	Attenuation (dB/cm/MHz)	Number of Cells
Growth 1 (G1)	9.4 ± 1.5	1565 ± 20	1.555 ± 0.014	993 ± 18	2.43 ± 0.03	1.20 ± 0.18	58
Growth 2 (G2)	11.4 ± 1.7	1572 ± 17	1.557 ± 0.011	991 ± 14	2.45 ± 0.03	1.05 ± 0.18	58
Metaphase	19.4 ± 2.5	1563 ± 13	1.537 ± 0.007	983 ± 10	2.40 ± 0.02	0.87 ± 0.18	58
Early Apoptotic	14.0 ± 2.1	1588 ± 18	1.542 ± 0.010	971 ± 13	2.45 ± 0.03	2.16 ± 0.40	58
Late Apoptotic	10.0 ± 1.6	1559 ± 31	1.540 ± 0.014	988 ± 22	2.40 ± 0.05	1.52 ± 0.36 (High Group) 0.56 ±0 .19 (Low Group)	58
Water[29]	—	1521	1.510	993	2.31	0.0014	—

increase in cell height from either the G1 or G2 phases to 14.0 ± 2.1 μm in early apoptosis. This is followed by a decrease in cell height as cells progress through apoptosis, to a value of 10.0 ± 1.6 μm for late apoptosis.

The speed of sound (**Fig. 2B**) through cells was statistically similar among cells in the proliferative cell cycle. In contrast, commitment to apoptosis from either G1 (1565 ± 20 m/s) or G2 (1572 ± 17 m/s) resulted in an increase in the speed of sound, reaching a value of 1588 ± 18 m/s in early apoptosis ($p < 0.001$). The speed of sound decreased to 1559 ± 31 m/s as early apoptotic cells progressed into late apoptosis.

The acoustic impedance (**Fig. 2C**) was statistically similar between G1 (1.555 ± 0.014 MRayls) and G2 (1.557 ± 0.011 MRayls) cells ($p > 0.05$). Progression into mitotic metaphase (1.537 ± 0.007 MRayls) from G2 or commitment to early apoptosis (1.542 ± 0.010 MRayls) from either G1 or G2 was marked by a decrease in the acoustic impedance ($p < 0.001$). Progression through apoptosis did not change the acoustic impedance significantly as cells entered late apoptosis (1.540 ± 0.014 MRayls).

Cellular density as assessed by ultrasound (**Fig. 2D**) around the nuclear region was found to be statistically similar between G1 (993 ± 18 kg/m^3) and G2 (991 ± 14 kg/m^3) cells, as well as between G2 and metaphase (983 ± 10 kg/m^3) cells. Notably, cells entering G1 following mitosis were observed to have a higher density around the nuclear region than metaphase cells. Commitment to apoptosis was marked by a decrease in the sound-derived density of the nuclear area in early apoptosis (971 ± 13 kg/m^3), followed by an increase to values significantly similar to that of G1 and G2 cells in late apoptosis (988 ± 22 kg/m^3)

The adiabatic bulk modulus (**Fig. 2E**) was determined to be statistically similar between G1 (2.43 ± 0.03 GPa) and G2 (2.45 ± 0.03 GPa) cells. Progression to metaphase (2.40 ± 0.02 GPa) from G2 featured a decrease in the adiabatic bulk modulus followed by an increase as cells returned to G1. Commitment to apoptosis through paclitaxel-caffeine treatment was not marked by a decrease until cells progressed significantly through the cell death program into Late Apoptosis (2.40 ± 0.05 GPa).

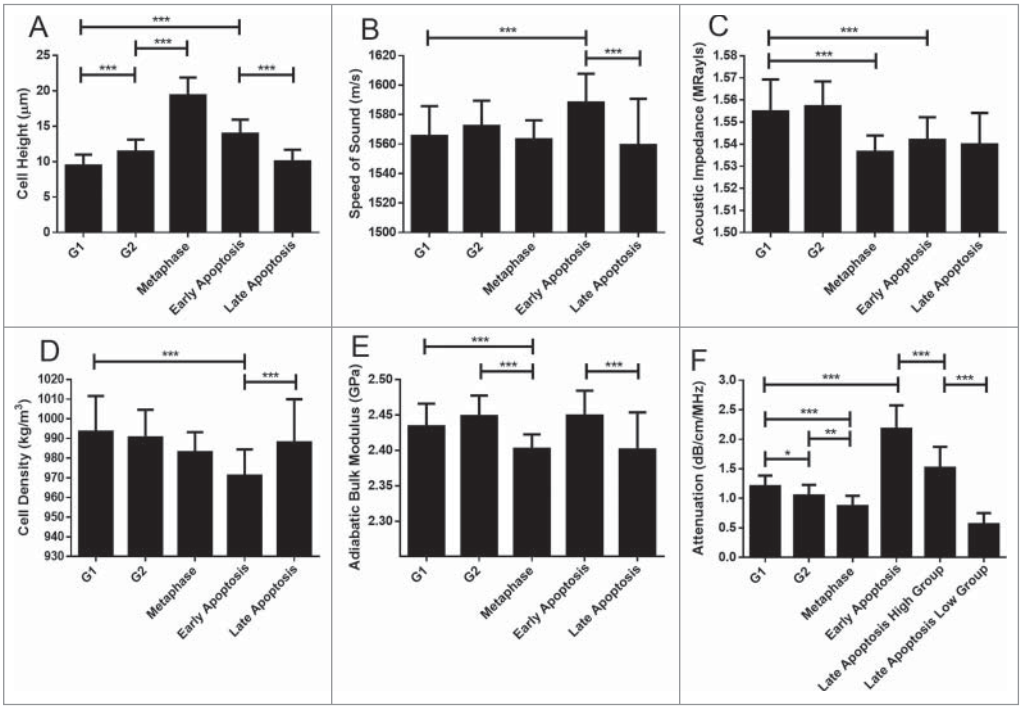

Figure 2. Cell properties as a function of cell state. Error bars represent standard deviations of 58 measurements. Black lines over top of the data represent comparison between groups, with the number of asterisks corresponding to a significance of difference. * $p \leq 0.05$; ** $p \leq 0.01$; *** $p \leq 0.001$. 58 cells were measured for each property.

Attenuation (**Fig. 2F**) was the only property whose differences were found to be statistically significant between all measured groups. A trend of decreasing attenuation was observed as cells progressed through the proliferative cell cycle: from 1.20 ± 0.18 dB/cm/MHz in G1 to 1.05 ± 0.18 dB/cm/MHz in G2 and lastly to 0.87 ± 0.18 dB/cm/MHz in metaphase. Commitment to apoptosis from either G1 or G2 was marked by a highly significant increase in the attenuation -up to 2.16 ± 0.40 in early apoptosis.

The ultrasound data from almost every measured group fit a standard Gaussian distribution, as depicted in **Fig. 3A** for metaphase cells. The exception was the late apoptosis group, which did not fit a standard Gaussian distribution. This histogram displayed a bimodal distribution, with no cells expressing attenuation values between 0.95 and 1.04 dB/cm/MHz (**Fig. 3**). The two groups, that we termed "Late Apoptosis – High Attenuation" and "Late Apoptosis – Low Attenuation" have attenuations of 1.52 ± 0.36 dB/cm/MHz and 0.56 ± 0.19 dB/cm/MHz ($p < 0.001$), and are therefore considered to be 2 distinct subgroups (**Fig. 3B**).

Discussion

Fluorescent imaging provided evidence that the correct cell phase had been assessed by acoustic microscopy. In addition, fluorescent imaging was used to distinguish morphological differences in different cell cycle phases, which correlates to changes in the scattering of acoustic waves and therefore allows this technology to classify cells.

The increase in cell height as MCF-7 cells progress from G1 to G2 correlate with an overall increase in cell size.[30] RO-3306 arrests cells on the G2 side of the G2/M transition[31] and so most G2-measured cells are at their maximum size prior to mitosis. Progression into mitosis features an additional increase in cell height as cells change from a flat adherent morphology to rounded.[28] In addition, the contact between mitotic cells and the substrate is reduced.[32] These factors likely contribute to the observed increase in cell height in the comparison of G2 interphase cells to metaphase cells. Apoptosis commitment features a similar phenotype of cellular rounding and partial detachment from the extracellular matrix,[33,34] leading to an increase in the cell height.The loss of cell height observed in the progression from early to late apoptosis can be attributed to the overall loss of cellular volume and content through the continual blebbing phenomenon and loss of membrane permeabilty.[35,36] Although both mitosis and apoptosis involve cell rounding due to partial detachment from the substrate, acoustic measurement of cell height may quickly discern cell growth from apoptosis, as cell undergoing the latter process will proceed to decrease cell height.

This study has demonstrated that increases in the speed of sound occur as viable cells enter early apoptosis, and therefore may contribute to the increased ultrasound backscatter observed in other studies.[37] Currently, it is difficult to determine the cell structures responsible for this observation. However, other studies have indicated that cells undergoing apoptosis feature changes in the elastic and viscous moduli,[8,38] which may have an impact on the sound speed.

The cytoskeleton is a major contributor to the mechanical properties of cells.[39] The microtubules of the cytoskeleton are proposed to be the main compressive load-bearing components in cells, and therefore play a major role in determining the cell's adiabatic bulk modulus - its resistance to compression.[40] This is consistent with the measurements that indicate a similar adiabatic bulk modulus for G1 and G2 cells, which have similar arrangements of microtubules between an intact nuclear envelope and plasma membrane. The decrease in the adiabatic bulk modulus for cells within metaphase may be due to the known change of actins, septins, and lamins from mechanical stress-bearing roles to alternate functions during mitosis, including cleavage furrow formation, extension of spindle fibers, and priming the nuclear envelope to reassemble post-mitosis.[41-43] Additionally, a study found that the microtubule network is rearranged in metaphase such that the load-bearing axis of microtubules is arranged parallel to the substratum[44] and therefore perpendicular to the axis of the cell for which the adiabatic bulk modulus measurement is taken. These factors, coupled with the absense of an intact nucleus[10] serving as a scaffold for the cytoskeleton via linkage proteins such as plectin and nesprin-3,[45] likely account for the lowered adiabatic bulk modulus for cells within metaphase.

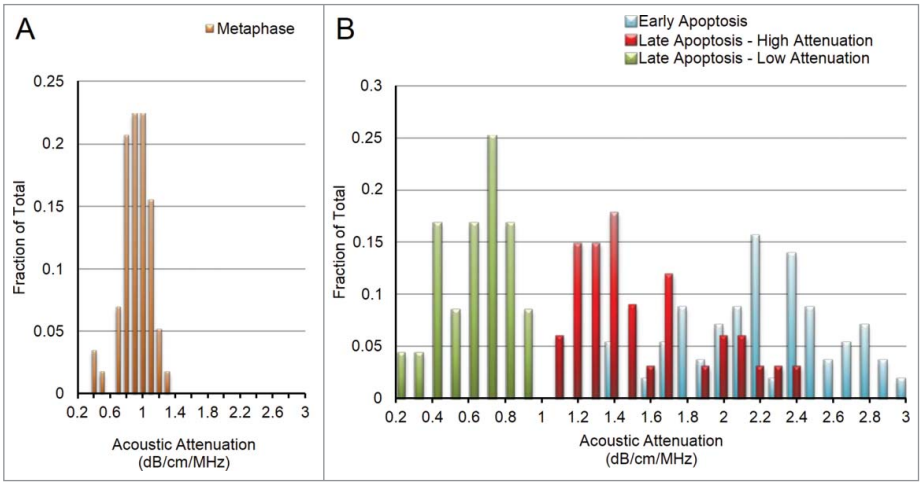

Figure 3. (**A**) With a single exception, all properties for all cell groups displayed approximate Gaussian curves, as above for attenuation in metaphase cells. (**B**) Attenuation for late apoptotic cells displayed a double-bell shaped distribution, indicating the existence of a "lower attenuation" subgroup (green) and a "higher attenuation" subgroup (blue). Early apoptotic histogram is seen in red to for easier visualization of the decrease in attenuation values as cells progress through apoptosis.

In contrast to mitosis, the early stages of apoptosis do not display a decrease in adiabatic bulk modulus despite sharing common intracellular events including the depolymerization of actins.[46] Recent studies have observed that the nuclear envelope remains intact in early apoptosis,[47] despite the proteolysis of lamin components. Microtubules have been found to display rapid assembly during early apoptosis[48] along with the maintenance of intermediate filaments,[49] which support the microtubule cytoarchitecture through cross talk.[50] The induction of apoptosis by the microtubule-stabilizing drug pacilitaxel[51] may have further contributed to the maintainance of the microtubule network, accounting for the lack of change in adiabatic bulk modulus relative to G1 and G2 cells. Much of this cytoskeletal stability disappears by the latter stages of apoptosis, with the nucleus being entirely collapsed and most nuclear anchoring protein–microtubule–intermediate filament linkages broken,[52] possibly accounting for the decrease in adiabatic bulk modulus observed for late apoptotic cells.

Attenuation was the only ultrasound parameter that could be used to differentiate between all measured phases of MCF-7 adenocarcinoma cells. At the frequency used in this study, attenuation is influenced by both absorption and scattering of the cell through which sound waves travel. The progressive decrease in attenuation as cells transition through the proliferative cell cycle into mitosis indicates that intracellular bodies are altered through the process such that there is a lesser degree of net absorption and scattering. The classical breakdown of the nucleus at the beginning of mitosis is marked by phosphorylation of nuclear lamins and the dissolution of the nuclear envelope,[53] followed by sequestration of both toward the cell periphery.[54-56] The endoplasmic reticulum has also been noted to be relocated in a similar manner.[11] With the absence of the nucleus and surrounding organelles as bodies to absorb and scatter ultrasound energy, the attenuation would be expected to decrease, as observed in this study. Geometric effects due to cellular rounding are unlikely to play an important role in these measurements, as early apoptotic cells, which share a rounded morphology with cells in metaphase, displayed the opposite trend. Commitment to apoptosis was marked by a large increase in attenuation. This is consistent with previous studies using HeLa[57] and MCF-7[24] cell lines, with the novel observation that these higher attenuation values are associated only with early apoptosis. It is not known what may account for this increase in attenuation. This trend may be the result of multiple intracellular changes which increase both the absorption and scattering of ultrasound signals, including the collapse of the cytokeratin network into aggregates,[58,59] the maintenance of an intact nuclear envelope as an absorbing body,[47,53] the fragmentation of the lamin cytoskeleton,[60] and the pronounced fragmentation of organelles such as the endoplasmic reticulum.[61]

Late apoptotic cells appeared sub-divided into 2 groups based on the measured attenuation. Both subgroups have significantly lower attenuation than early apoptosis, with the "high attenuation" subgroup approaching values closer to those of G1 and G2 and the "low attenuation" subgroup displaying an average value lower than even that of metaphase cells. Notably, the work of Span et al.[62] has also observed 2 subgroups in late-apoptosis based on flow cytometric analysis of Annexin V and propidium iodide. It is uncertain whether these 2 subgroups reflect different sub-stages in the late apoptotic program, or whether they reflect different end-states the cells might achieve. Despite these unknowns, acoustic microscopy is capable of identifying such distinctions, demonstrating that non-invasive measurement of physical and mechanical properties can reveal additional information and uncover new questions in the study of cellular death.

The capacity for acoustic microscopy to noninvasively characterize cells according to changes to their physical properties provides a label-free means of studying cell dynamics over extended time periods. Moreover, the results are also used in algorithms designed to classify biological samples in a flow system using ultra high frequency backscattered waves – the acoustic equivalent to modern flow cytometry technology.[63,64]

Conclusion

Acoustic microscopy was used to evaluate the state of live cells in a manner that avoids the use of chemical agents or genetic engineering. These measurements allowed the characterization of physical and mechanical property changes as cells progress through both the proliferative cell cycle and the apoptotic program. The measurements were done on 290 cells and statistically significant differences were measured. It was found that ultrasound attenuation was the only parameter that could be used to discriminate all cell states identified in this work. Additionally, the decrease in the adiabatic bulk modulus from 2.43 ± 0.03 GPa in G1 to 2.40 ± 0.02 GPa in metaphase as well as the decrease in cell density by at least $8 kg/m^3$ from G1 to early apoptosis can serve as an auxiliary set of observations to make a distinction between cells continuing to proliferate versus cells undergoing death, respectively. Increases in attenuation for apoptotic cells by more than 80% have been attributed to only early apoptosis, answering previous questions concerning the timing of the observed increase. Finally, new trends including the decreasing attenuation trend for proliferating cells, and the appearance of 2 subgroups within late apoptosis are all promising fields of further research in bettering our understanding of cellular life and death.

Methods

Acoustic Microscopy

Experiments were performed using the SASAM acoustic microscope (Kibero GmBH Saarbrücken, Germany, http://www.kibero.com/html/products.htm). The microscope consists of an Olympus IX81 optical microscope combined with an acoustic module. The ultrasound transducer was positioned above the sample stage, allowing for simultaneous optical, fluorescent and acoustic visualization of the sample. The acoustic module was rotated along a column to allow for fast switching with an optical condenser for phase contrast imaging. Ultrasound pulses were generated by a 300 MHz monocycle pulse

generator at a 125 kHz pulse repetition frequency, and the echoes were amplified by a 40-dB amplifier and digitized at 8 GS/s (Agilent DC252, http://cp.literature.agilent.com/litweb/pdf/5989-9190EN.pdf). The 375 MHz transducer had a 30° semi-aperture angle and a −6dB bandwidth of 42%.[26] All samples were measured at a constant temperature of 36°C.

The acoustic transducer remained stationary during measurements, the cells were scanned by moving the microscope stage using a microstepper system (Corvus, http://www.pimicos.com/web2/en/1,2,040,smc_corvus.html) This system was coupled with a programmed coordinate module, allowing for the administration of specific coordinates to measured cells relative to an arbitrary origin. All measurements were performed using a 375MHz central frequency transducer over the nuclear region of all cells. Focus positioning was confirmed through Hoescht 33342 staining of DNA chromatin. A step size of 1μm over a range of ±40 μm about the cell-glass substrate interface was used for measurements axially through the cell (V(z) curves). All measurements were averaged with 100 signals to improve the signal-to-noise ratio.

Cell culture

MCF-7 breast cancer cells (ATCC, http://www.atcc.org/products/all/HTB-22.aspx) were cultured in Dublecco's modified Eagle's medium (DMEM) cell culture medium with 10% fetal bovine serum (FBS) and 1% Penicillin-Streptomycin (Pen-Strep) solution (growth media). Cells were incubated at 37°C with 5% CO_2 and were passaged every 3–4 d at ~50–60% confluence to maintain exponential growth. Cells were dissociated from their flasks via trypsin (0.025%, Gibco, http://www.invitrogen.com/site/us/en/home/Products-and-Services/Applications/Cell-Culture/Mammalian-Cell-Culture/reagents/Trypsin/Trypsin.html) and transferred to Lab-Tek II chambers (Nunc, http://www.thermoscientific.com/ecomm/servlet/productsdetail_11152___11953123_-1), where they were grown for a period of 48 hours before use.

G1 and G2 Cells

After 48 hours growth in Lab-Tek II chambers, growth media was aspirated and replaced with new growth media supplemented with stage-arresting drug. MCF-7 cells were arrested in G1 using Lovastatin (20 μM, http://www.sigmaaldrich.com/catalog/product/sigma/m2147)[65] for 33 hours, or G2 by treatment with RO-3306 (9 μM, http://www.emdmillipore.com/life-science-research/cdk1-inhibitor-iv-ro-3306-calbiochem/EMD_BIO-217699/p_BI6b.s1LTrAAAAEWx2EfVhTm)[6] for 24 hours. Cells remained in contact with arresting-agent-containing medium throughout measurement. Measurements for G1 and G2 cells were performed under minimal light exposure due to the photosensitive nature of the phase-arresting compounds.

Immediately following the measurements, cells were fixed either in 100% methanol (Sigma Aldrich, http://www.sigmaaldrich.com/catalog/product/sial/179337) for G1 cells or 99% ethanol (Sigma Aldrich, http://www.sigmaaldrich.com/catalog/product/sial/676829) for G2 cells, and stored at −20°C overnight. Cells were permeabilized with 0.25% v/v Triton X100 in PBS for 10 minutes cells were then incubated with 3% w/v BSA and 0.1% v/v primary mouse anti-cyclin D1 antibody (BD PharMingen, http://www.bdbiosciences.com/external_files/pm/doc/tds/cell_bio/live/web_enabled/14561C_554181.pdf) or 0.1% v/v primary mouse anti-cyclin B1 antibody (BD PharMingen, http://www.bdbiosciences.com/external_files/pm/doc/tds/cell_bio/live/web_enabled/14541A_554176.pdf) to confirm G1 and G2, respectively. After 2 hour incubation at 4°C, samples were washed and incubated with 3% w/v BSA, Hoescht DNA fluorescent stain (2 μM) and 0.5% v/v secondary Alexa-Fluor 488 goat anti-mouse antibody (Invitrogen, http://products.invitrogen.com/ivgn/product/A11001) at 4°C for 24 hours. Following immunofluorescence staining, previously measured cells were relocated using the sample stage coordinate system to ensure that all measured cells were in the desired phase.

Metaphase Cells

48 hours post-transfer to Lab-Tek II chambers, growth medium was aspirated and replaced with growth media containing Hoescht DNA fluorescent stain (2 μM). A combination of a rounded phenotype under bright field and aligned chromosomes visualized under fluorescence were used to identify metaphase cells for measurements.

Apoptotic Cells

48 hours after transfer to Lab-Tek II chambers, the medium was replaced with DMEM (no FBS / no Pen-Strep solution) supplemented with 3mg/ml caffeine and 20ng/ml paclitaxel and incubated for 18 to 20 hours to induce apoptosis.[66] Hoescht DNA fluorescent stain (2 μM), Annexin V (Biovision Apoptosis Kit, http://www.biovision.com/annexin-v-fitc-apoptosis-kit-2645.html) phosphatidylserine stain (0.6 μg/mL), and propidium iodide (Biovision Apoptosis Kit) nucleotide stain (6 μM) were then added to the apoptosis-inducing medium so as to not disturb apoptotic cells that were poorly adhered to the chambers. These fluorescent markers were incubated with the cells for 10 minutes prior to measurement. Acoustic measurements from cells in both early and late apoptosis were then recorded. Cells with visible blebbing and a rounded phenotype under bright field imaging, along with positive fluorescent staining for Annexin V and negative for propidium iodide, were identified to be in early apoptosis. Cells fluorescently staining positive for both Annexin V and propidium iodide were identified to be in late apoptosis.

Statistical analyses

A total of 290 cells were measured, 58 from each of the cell phases studied. Comparisons between values for cell properties were carried out using single factor ANOVA followed by Tukey Post Hoc analyses in Graphpad Instat 3 (GraphPad Software, http://www.graphpad.com/scientific-software/instat). Of the statistically significant differences observed, only differences between cell phases occurring in sequential order (i.e early apoptosis to late apoptosis, but not G1 to late apoptosis) were taken into account.

Disclosure of Potential Conflicts of Interest

No potential conflicts of interest were disclosed.

Acknowledgments

We thank Lauren Wirtzfeld (Ryerson University) for her assistance with statistical analyses and Arthur Worthington (Ryerson University) for his technical support during the course of these experiments.

Funding

This research was undertaken, in part, thanks to funding from the Natural Sciences and Engineering Research Council (grant #216986–2012) The Terry Fox New Frontiers Program Project Grant in Ultrasound and MRI for Cancer Therapy (#1034), and Ryerson University. Funding to purchase the acoustic microscopy equipment was provided by the Canada Foundation for Innovation, the Ontario Ministry of Research and Innovation, and Ryerson University.

References

1. Pucci B, Kasten M, Giordano A. Cell cycle and apoptosis. Neoplasia 2000; 2:291–9; PMID:11005563; http://dx.doi.org/10.1038/sj.neo.7900101
2. Sesso A, Fujiwara DT, Jaeger M, Jaeger R, Li TC, Monteiro MM, Correa H, Ferreira MA, Schumacher RI, Belisário J, et al. Structural elements common to mitosis and apoptosis. Tissue Cell 1999; 31:357–71; PMID:10481307; http://dx.doi.org/10.1054/tice.1999.0042
3. Juan G, Hernando E, Cordon-Cardo C. Separation of live cells in different phases of the cell cycle for gene expression analysis. Cytometry 2002; 49:170–5; PMID:12454980; http://dx.doi.org/10.1002/cyto.10173
4. Bhatt RI, Brown MD, Hart CA, Gilmore P, Ramani VA, George NJ, Clarke NW. Novel method for the isolation and characterisation of the putative prostatic stem cell. Cytometry A 2003; 54:89–99; PMID:12879455; http://dx.doi.org/10.1002/cyto.a.10058
5. Easwaran HP, Leonhardt H, Cardoso MC. Cell cycle markers for live cell analyses. Cell Cycle 2005; 4:453–5; PMID:15701967; http://dx.doi.org/10.4161/cc.4.3.1525
6. Sadikovic B, Al-Romaih K, Squire JA, Zielenska M. Cause and consequences of genetic and epigenetic alterations in human cancer. Curr Genomics 2008; 9:394–408; PMID:19506729; http://dx.doi.org/10.2174/138920208785699580
7. González-Cruz RD, Fonseca VC, Darling EM. Cellular mechanical properties reflect the differentiation potential of adipose-derived mesenchymal stem cells. Proc Natl Acad Sci USA 2012; 109:E1523–9; http://dx.doi.org/10.1073/pnas.1120349109
8. Pelling AE, Veraitch FS, Chu CP, Mason C, Horton MA. Mechanical dynamics of single cells during early apoptosis. Cell Motil Cytoskeleton 2009; 66:409–22; PMID:19492400; http://dx.doi.org/10.1002/cm.20391
9. Nelson D, Ye X, Hall C, Santos H, Ma T, Kao G, Yen T, Harper J, Adams P. Coupling of DNA Synthesis and Histone Synthesis in S Phase Independent of Cyclin/cdk2 Activity. Mol Cell Biol 2002; 22:7459–7472; PMID:12370293; http://dx.doi.org/10.1128/MCB.22.21.7459-7472.2002
10. Georgatos SD, Pyrpasopoulou A, Theodoropoulos PA. Nuclear envelope breakdown in mammalian cells involves stepwise lamina disassembly and microtubule-drive deformation of the nuclear membrane. J Cell Sci 1997; 110 (Pt 17):2129–40; PMID:9378763
11. Stewart MP, Helenius J, Toyoda Y, Ramanathan SP, Muller DJ, Hyman AA. Hydrostatic pressure and the actomyosin cortex drive mitotic cell rounding. Nature 2011; 469:226–30; PMID:21196934; http://dx.doi.org/10.1038/nature09642
12. Lu L, Ladinsky MS, Kirchhausen T. Cisternal organization of the endoplasmic reticulum during mitosis. Mol Biol Cell 2009; 20:3471–80; PMID:19494040; http://dx.doi.org/10.1091/mbc.E09-04-0327
13. Chong ZZ, Kang J-QQ, Maiese K. Essential cellular regulatory elements of oxidative stress in early and late phases of apoptosis in the central nervous system. Antioxid Redox Signal 2004; 6:277–87; PMID:15025929; http://dx.doi.org/10.1089/152308604322899341
14. Saraste A, Pulkki K. Morphologic and biochemical hallmarks of apoptosis. Cardiovasc Res 2000; 45:528–37; PMID:10728374; http://dx.doi.org/10.1016/S0008-6363(99)00384-3
15. Coleman ML, Sahai EA, Yeo M, Bosch M, Dewar A, Olson MF. Membrane blebbing during apoptosis results from caspase-mediated activation of ROCK I. Nat Cell Biol 2001; 3:339–45; PMID:11283606; http://dx.doi.org/10.1038/35070009
16. Kole TP, Tseng Y, Wirtz D. Intracellular microrheology as a tool for the measurement of the local mechanical properties of live cells. Methods Cell Biol 2004; 78:45–64; PMID:15646615; http://dx.doi.org/10.1016/S0091-679X(04)78003-6
17. Costa KD. Imaging and probing cell mechanical properties with the atomic force microscope. Methods Mol Biol 2006; 319:331–61; PMID:16719364; http://dx.doi.org/10.1007/978-1-59259-993-6_17
18. Zahalak GI, McConnaughey WB, Elson EL. Determination of cellular mechanical properties by cell poking, with an application to leukocytes. J Biomech Eng 1990; 112:283–94; PMID:2214710; http://dx.doi.org/10.1115/1.2891186
19. Thoumine O, Ott A. Time scale dependent viscoelastic and contractile regimes in fibroblasts probed by microplate manipulation. J Cell Sci 1997; 110 (Pt 17):2109–16; PMID:9378761
20. Vliet K, Bao G, Suresh S. The biomechanics toolbox: experimental approaches for living cells and biomolecules. Acta Materialia 2003; 51:58815905
21. Liner A, Winkelhaus S, Hauser M. Acoustic imaging of the mitotic spindle in dividing XTH2-cells. J Acoust Soc Am 1994; 95:523–8
22. Kolios MC, Czarnota GJ, Lee M, Hunt JW, Sherar MD. Ultrasonic spectral parameter characterization of apoptosis. Ultrasound Med Biol 2002; 28:589–97; PMID:12079696; http://dx.doi.org/10.1016/S0301-5629(02)00492-1
23. Czarnota GJ, Kolios MC, Abraham J, Portnoy M, Ottensmeyer FP, Hunt JW, Sherar MD. Ultrasound imaging of apoptosis: high-resolution non-invasive monitoring of programmed cell death in vitro, in situ and in vivo. Br J Cancer 1999; 81:520–7; PMID:10507779; http://dx.doi.org/10.1038/sj.bjc.6690724
24. Strohm EM, Czarnota GJ, Kolios MC. Quantitative measurements of apoptotic cell properties using acoustic microscopy. IEEE Trans Ultrason Ferroelectr Freq Control 2010; 57:2293–304; PMID:20889417; http://dx.doi.org/10.1109/TUFFC.2010.1690
25. Briggs A, Kolosov O. Acoustic microscopy. 2nd rev. ed. New York: Oxford University Press; 2009; 380 p.
26. Weiss EC, Anastasiadis P, Pilarczyk G, Lemor RM, Zinin PV. Mechanical properties of single cells by high-frequency time-resolved acoustic microscopy. IEEE Trans Ultrason Ferroelectr Freq Control 2007; 54:2257–71; PMID:18051160; http://dx.doi.org/10.1109/TUFFC.2007.530
27. Dusek RL, Godsel LM, Chen F, Strohecker AM, Getsios S, Harmon R, Müller EJ, Caldelari R, Cryns VL, Green KJ. Plakoglobin deficiency protects keratinocytes from apoptosis. J Invest Dermatol 2007; 127:792–801; PMID:17110936; http://dx.doi.org/10.1038/sj.jid.5700615
28. Kok SH, Chui CH, Lam WS, Chen J, Lau FY, Cheng GY, Wong RS, Lai PP, Leung TW, Tang JC, et al. Apoptotic activity of a novel synthetic cantharidin analogue on hepatoma cell lines. Int J Mol Med 2006; 17:945–9; PMID:16596285
29. Meister U, Ohnesorge B, Körner D, Boevé M. Evaluation of ultrasound velocity in enucleated equine aqueous humor, lens and vitreous body. BMC Vet Res 2014; 10:250; PMID:25312851; http://dx.doi.org/10.1186/s12917-014-0250-3
30. Sorenson CM, Barry MA, Eastman A. Analysis of events associated with cell cycle arrest at G2 phase and cell death induced by cisplatin. J Natl Cancer Inst 1990; 82:749–55; PMID:1691303; http://dx.doi.org/10.1093/jnci/82.9.749
31. Vassilev LT, Tovar C, Chen S, Knezevic D, Zhao X, Sun H, Heimbrook DC, Chen L. Selective small-molecule inhibitor reveals critical mitotic functions of human CDK1. Proc Natl Acad Sci USA 2006; 103:10660–5; PMID:16818887; http://dx.doi.org/10.1073/pnas.0600447103
32. Baker J, Garrod D. Epithelial cells retain junctions during mitosis. J Cell Sci 1993; 104 (Pt 2):415–25; PMID:7685036
33. Ndozangue-Touriguine O, Hamelin J, Bréard J. Cytoskeleton and apoptosis. Biochem Pharmacol 2008; 76:11–8; PMID:18462707; http://dx.doi.org/10.1016/j.bcp.2008.03.016
34. Andrade R, Crisol L, Prado R, Boyano MD, Arluzea J, Aréchaga J. Plasma membrane and nuclear envelope integrity during the blebbing stage of apoptosis: a time-lapse study. Biol Cell 2010; 102:25–35; http://dx.doi.org/10.1042/BC20090077
35. Henson PM, Tuder RM. Apoptosis in the lung: induction, clearance and detection. Am J Physiol Lung Cell Mol Physiol 2008; 294:L601–11; PMID:18178675; http://dx.doi.org/10.1152/ajplung.00320.2007
36. Edinger AL, Thompson CB. Death by design: apoptosis, necrosis and autophagy. Curr Opin Cell Biol 2004; 16:663–9; PMID:15530778; http://dx.doi.org/10.1016/j.ceb.2004.09.011
37. Taggart LR, Baddour RE, Giles A, Czarnota GJ, Kolios MC. Ultrasonic characterization of whole cells and isolated nuclei. Ultrasound Med Biol 2007; 33:389–401; PMID:17257739; http://dx.doi.org/10.1016/j.ultrasmedbio.2006.07.037
38. El Kaffas A, Bekah D, Rui M, Kumaradas JC, Kolios MC. Investigating longitudinal changes in the mechanical properties of MCF-7 cells exposed to paclitaxol using particle tracking microrheology. Phys Med Biol 2013; 58:923–36; PMID:23340402; http://dx.doi.org/10.1088/0031-9155/58/4/923
39. Gardel ML, Kasza KE, Brangwynne CP, Liu J, Weitz DA. Chapter 19: Mechanical response of cytoskeletal networks. Methods Cell Biol 2008; 89:487–519; PMID:19118688; http://dx.doi.org/10.1016/S0091-679X(08)00619-5
40. Ingber DE. Tensegrity I. Cell structure and hierarchical systems biology. J Cell Sci 2003; 116:1157–73; PMID:12615960; http://dx.doi.org/10.1242/jcs.00359
41. Heng Y-WW, Koh C-GG. Actin cytoskeleton dynamics and the cell division cycle. Int J Biochem Cell Biol 2010; 42:1622–33; PMID:20412868; http://dx.doi.org/10.1016/j.biocel.2010.04.007

42. Joo E, Surka MC, Trimble WS. Mammalian SEPT2 is required for scaffolding nonmuscle myosin II and its kinases. Dev Cell 2007; 13:677–90; PMID:17981136; http://dx.doi.org/10.1016/j.devcel.2007.09.001
43. Gruenbaum Y, Margalit A, Goldman RD, Shumaker DK, Wilson KL. The nuclear lamina comes of age. Nat Rev Mol Cell Biol 2005; 6:21–31; PMID:15688064; http://dx.doi.org/10.1038/nrm1550
44. Toyoshima F, Nishida E. Integrin-mediated adhesion orients the spindle parallel to the substratum in an EB1- and myosin X-dependent manner. EMBO J 2007; 26:1487–98; PMID:17318179; http://dx.doi.org/10.1038/sj.emboj.7601599
45. Wilhelmsen K, Litjens SH, Kuikman I, Tshimbalanga N, Janssen H, Bout I, Raymond K, Sonnenberg A. Nesprin-3, a novel outer nuclear membrane protein, associates with the cytoskeletal linker protein plectin. J Cell Biol 2005; 171:799–810; PMID:16330710; http://dx.doi.org/10.1083/jcb.200506083
46. McCarthy NJ, Whyte MK, Gilbert CS, Evan GI. Inhibition of Ced-3/ICE-related proteases does not prevent cell death induced by oncogenes, DNA damage, or the Bcl-2 homologue Bak. J Cell Biol 1997; 136:215–27; PMID:9008715; http://dx.doi.org/10.1083/jcb.136.1.215
47. Wong C-HH, Chan H, Ho C-YY, Lai S-KK, Chan K-SS, Koh C-GG, Li H-YY. Apoptotic histone modification inhibits nuclear transport by regulating RCC1. Nat Cell Biol 2009; 11:36–45; PMID:19060893; http://dx.doi.org/10.1038/ncb1810
48. Moss DK, Betin VM, Malesinski SD. A novel role for microtubules in apoptotic chromatin dynamics and cellular fragmentation. J Cell Sci 2006; 119:2362–74; PMID:16723742; http://dx.doi.org/10.1242/jcs.02959
49. Coulombe PA, Wong P. Cytoplasmic intermediate filaments revealed as dynamic and multipurpose scaffolds. Nat Cell Biol 2004; 6:699–706; PMID:15303099; http://dx.doi.org/10.1038/ncb0804-699
50. Chang L, Goldman RD. Intermediate filaments mediate cytoskeletal crosstalk. Nat Rev Mol Cell Biol 2004; 5:601–13; PMID:15366704; http://dx.doi.org/10.1038/nrm1438
51. Gangemi R, Tiso M, Marchetti C, Severi AB. Taxol cytotoxicity on human leukemia cell lines is a function of their susceptibility to programmed cell death. Cancer Chemother Pharmacol 1995; 36:285–92; http://dx.doi.org/10.1007/BF00686187
52. Leung CL, Green KJ, Liem R. Plakins: a family of versatile cytolinker proteins. Trends Cell Biol 2002; 12:37–45; PMID:11854008; http://dx.doi.org/10.1016/S0962-8924(01)02180-8
53. Tsai MY, Wang S, Heidinger JM, Shumaker DK. A Mitotic Lamin B Matrix Induced by RanGTP Required for Spindle Assembly. Science 2006; 311:1887–93; PMID:16543417; http://dx.doi.org/10.1126/science.1122771
54. Jost E, Lepper K, Högner, D, Zimmer A. Redistribution of nuclear lamins in mitotic cells. Biol Cell 1986; 57:111–26; PMID:2948591; http://dx.doi.org/10.1111/j.1768-322X.1986.tb00468.x
55. Chaly N, Bladon T, Setterfield G, Little JE, Kaplan JG, Brown DL. Changes in distribution of nuclear matrix antigens during the mitotic cell cycle. J Cell Biol 1984; 99:661–71; PMID:6378926; http://dx.doi.org/10.1083/jcb.99.2.661
56. Margalit A, Vlcek S, Gruenbaum Y. Breaking and making of the nuclear envelope. J Cell Biochem 2005; 95:454–65; PMID:15832341; http://dx.doi.org/10.1002/jcb.20433
57. Brand S, Weiss EC, Lemor RM, Kolios MC. High frequency ultrasound tissue characterization and acoustic microscopy of intracellular changes. Ultrasound Med Biol 2008; 34:1396–407; PMID:18439747; http://dx.doi.org/10.1016/j.ultrasmedbio.2008.01.017
58. Lee JC, Schickling O, Stegh AH, Oshima RG. DEDD regulates degradation of intermediate filaments during apoptosis. J Cell Biol 2002; 158:1051–66; PMID:12235123; http://dx.doi.org/10.1083/jcb.200112124
59. Schutte B, Henfling M, Kölgen W, Bouman M. Keratin 8/18 breakdown and reorganization during apoptosis. Exp Cell Res 2004; 294:11–26; PMID:15194421; http://dx.doi.org/10.1016/j.yexcr.2004.02.019
60. Oberhammer FA, Hochegger K, Fröschl G, Tiefenbacher R, Pavelka M. Chromatin condensation during apoptosis is accompanied by degradation of lamin A+B, without enhanced activation of cdc2 kinase. J Cell Biol 1994; 126:827–37; PMID:8051209; http://dx.doi.org/10.1083/jcb.126.4.827
61. Taylor RC, Cullen SP, Martin SJ. Apoptosis: controlled demolition at the cellular level. Nat Rev Mol Cell Biol 2008; 9:231–41; PMID:18073771; http://dx.doi.org/10.1038/nrm2312
62. Span LF, Pennings AH, Vierwinden G, Boezeman JB, Raymakers RA, Witte T de. The dynamic process of apoptosis analyzed by flow cytometry using Annexin-V/propidium iodide and a modified in situ end labeling technique. Cytometry 2002; 47:24–31; PMID:11774346; http://dx.doi.org/10.1002/cyto.10028
63. Strohm, EM, MC Kolios, D Hwang, B-U Moon, SS Tsai. Development of a microfluidic device with integrated high frequency ultrasound probe for particle characterization. IEEE Symp. 2014; 1960–63; http://dx.doi.org/10.1109/ULTSYM.2014.0487
64. Strohm EM, Kolios MC. Classification of blood cells and tumor cells using label-free ultrasound and photoacoustics. Cytometry A 2015; PMID:26079610
65. Sangjun S Jong E, de Nijmeijer S, Mutarapat T, Ruchirawat S, Berg M, van den Duursen MB van. Induction of cell cycle arrest in human MCF-7 breast cancer cells by cis-stilbene derivatives related to VIOXX. Toxicol Lett 2009; 186:115–22; PMID:19429232; http://dx.doi.org/10.1016/j.toxlet.2009.01.017
66. Saunders DE, Lawrence WD, Christensen C, Wappler NL, Ruan H, Deppe G. Paclitaxel-induced apoptosis in MCF-7 breast-cancer cells. Int J Cancer 1997; 70:214–20; PMID:9009163; http://dx.doi.org/10.1002/(SICI)1097-0215(19970117)70:2%3c214::AID-IJC13%3e3.0.CO;2-I